Taylor & Francis
Taylor & Francis Group

Structure and Infrastructure Engineering
Maintenance, Management, Life-Cycle Design and Performance

ISSN: (Print) (Online) Journal homepage: https://www.tandfonline.com/loi/nsie20

Evaluation of intensity measure performance in regional seismic risk assessment of reinforced concrete bridge inventories

Andres Abarca, Ricardo Monteiro, Gerard O'Reilly, Elisa Zuccolo & Barbara Borzi

To cite this article: Andres Abarca, Ricardo Monteiro, Gerard O'Reilly, Elisa Zuccolo & Barbara Borzi (2021): Evaluation of intensity measure performance in regional seismic risk assessment of reinforced concrete bridge inventories, Structure and Infrastructure Engineering, DOI: 10.1080/15732479.2021.1979599

To link to this article: https://doi.org/10.1080/15732479.2021.1979599

Published online: 21 Sep 2021.

STRUCTURE AND INFRASTRUCTURE ENGINEERING
https://doi.org/10.1080/15732479.2021.1979599

Evaluation of intensity measure performance in regional seismic risk assessment of reinforced concrete bridge inventories

Andres Abarca[a], Ricardo Monteiro[a], Gerard O'Reilly[a], Elisa Zuccolo[b] and Barbara Borzi[b]

[a]Centre for Training and Research on Reduction of Seismic Risk (ROSE Centre), University School for Advanced Studies (IUSS) of Pavia, Pavia, Italy; [b]Department of Risk Scenarios, European Centre for Training and Research in Earthquake Engineering (EUCENTRE), Pavia, Italy

ABSTRACT

Seismic risk assessment requires fragility functions derived using non-linear time-history analysis with earthquake records compatible with the site hazard and characterised via a suitable intensity measure (IM), which poses a challenge given the wide variety of structural characteristics found in bridge inventories. Given the lack of consensus on a suitable IM, regional studies often use peak ground acceleration (PGA), which despite being recognized as a poor indicator of structural performance, has persisted in earthquake response characterisation. Average spectral acceleration (AvgSa) has recently gained popularity since it describes earthquake intensity over a range of pertinent periods of vibration; however, its suitability as an IM has not been demonstrated on real bridge inventories with a wide variety of structural characteristics. In this study, hazard-consistent records selected for both PGA and AvgSa are used to evaluate the response of a large inventory of existing bridges with varying structural characteristics, from the Italian roadway network. The results indicate that AvgSa is a more accurate IM compared to PGA when applied to the regional assessment of RC bridges.

ARTICLE HISTORY
Received 19 January 2021
Revised 21 April 2021
Accepted 28 June 2021

KEYWORDS
Regional seismic risk; bridges; intensity measure; average spectral acceleration; ground motion record selection; road network; infrastructure assessment

1. Introduction

In recent years, regional seismic risk assessment has seen a growing interest as a tool for stakeholders to quantify the expected performance of infrastructure inventories. Multiple applied research projects, such as ITERATE (DG-ECHO European Commission, 2017) or INFRA-NAT (DG-ECHO European Commission, 2018), have been developed where georeferenced databases of buildings and bridges are linked to seismic hazard and structural vulnerability models, enabling the development of risk maps for large regional areas, giving stakeholders access to useful information for efficient resource allocation and emergency management.

State-of-the-art seismic risk assessment requires the use of fragility functions typically derived via non-linear time-history analysis (NLTHA). This is done using earthquake records that are both: a) compatible with the seismic hazard and, b) characterized via an intensity measure (IM) suitable for the structures to be analysed. The latter condition is typically achieved by performing the record selection procedure with an IM that minimises the dispersion in the observed structural behaviour.

For the case of individual building structures, the use of the spectral acceleration at the fundamental period, $Sa(T_1)$, is a typical choice for the IM, which has proven to minimize the dispersion in the response of a structure to multiple ground motions with the same IM level. This option is based on the notion that the first mode response tends to govern the performance of most regular buildings with short to medium height. However, in the case of multi-span bridges or inventories with multiple classes of structures, no single period of vibration can be typically chosen to characterise the entire structural behaviour thus no clear answer exists on how to efficiently choose an IM.

Some studies have been conducted to address this issue, specifically investigating the impact of the choice of the IM on the development of fragility curves for bridges. Earlier work by Padgett, Nielson, and DesRoches (2008) concluded, using a limited number of bridge configurations, that peak ground acceleration (PGA) is the optimal choice for portfolio analysis since it provides adequate results and does not require consideration of the dynamic characteristics of the inventory.

More recent accounts (Monteiro, Zelaschi, Silva, & Pinho, 2019) have determined that some IMs such as peak ground velocity (PGV) and Fajfar index (I_v) show a better performance in comparison to PGA, however, they do not completely disqualify the use of the latter and recognize the advantages of its widespread availability and popularity amongst practitioners.

Reaching a consensus on the choice for an optimal IM for analytical fragility calculations remains an open challenge (Silva et al., 2019) and, therefore, recent regional studies have been many times performed in terms of PGA (Borzi et al., 2015; Carozza, Jalayer, Miano, & Manfredi, 2017) or spectral acceleration at 1 second (Sa_{1s}) as popularized by HAZUS (Porter, 2009), not because of their proven accuracy, but because of its convenience as IMs that are readily

CONTACT Ricardo Monteiro ricardo.monteiro@iusspavia.it University School for Advanced Studies (IUSS) of Pavia, Piazza della Vittoria n.15, 27100 Pavia, Italy

available in hazard calculations in most regional contexts. More recently, average spectral acceleration (AvgSa) (Eads, Miranda, & Lignos, 2015) has gained popularity as a promising alternative, given that it describes ground motion intensity in terms of the geometric mean of spectral demand over a range of pertinent periods of vibration. Some recent research has shown encouraging results for its use in portfolio assessment of structures (Kohrangi, Bazzurro, Vamvatsikos, & Spillatura, 2017) and specifically for bridges (O'Reilly & Monteiro, 2019), however, its claims as an efficient IM have not been yet verified on real inventories of bridges with a wide variety of structural characteristics.

In this study, sets of 270 bi-directional hazard-consistent records (i.e., 30 records at 9 intensities) were selected for PGA and AvgSa and used to evaluate the response, through NLTHA, of a case study inventory of 163 existing bridges with a wide variety of structural characteristics, representative of the Italian roadway network. Given the computational effort derived from such a large selection of records and case-study structures, the selection of intensity measures was restricted to the two previously mentioned only; while this could be seen a limitation of the present study, the intention is to compare the more novel AvgSa option to the more traditional and widely used option of PGA that has also proven an adequate performance for regional applications as mentioned previously.

To address the aforementioned gap related to the choice of a proper IM in bridge inventories, the results from such an extensive analysis campaign were scrutinised using several performance metrics that evaluate the statistical and behavioural performance of the entire set from an individual and taxonomy-based perspective with the aim of quantifying the impact of the choice of IM in the results typically obtained in regional risk assessment of bridge inventories.

Beyond the comparison between the use of the two aforementioned IMs (PGA and AvgSa) in bridge portfolio risk assessment, this work describes in detail the application of a state-of-the-art methodology for regional seismic risk assessment of bridges and, furthermore, the analysis of the results permits to gain insights into some practical questions that may arise when performing regional analysis of bridges, such as the applicability of taxonomy-based fragility curves for the calculation of risk assessment results and the mechanisms that govern the exceedance of the types of bridges analysed.

2. Methodology

The adopted methodology, shown schematically in Figure 1, consists of initially processing the database of existing bridges to create a numerical structural model of each of the 163 bridges available. These models were used to perform a preliminary analysis to determine the structural modal information used to define a representative period range for the computation of the AvgSa IM. This information is then combined with a probabilistic seismic hazard analysis (PSHA) performed at a specific site in Italy, taken as characteristic of the seismicity of the area where the bridge inventory is located. Both these results, concerning the definition of the period range of interest and the hazard conditions of the site, are used to perform a hazard-consistent record selection for both PGA and AvgSa in the selected period range, leading to a set of 30 bi-directional earthquake records for return periods of 30, 50, 98, 224, 475, 975, 2475, 4995 and 9975 years, hence, a total of 270 ground motion records for each IM. These records are then used to perform NLTHA on each of the 163 bridge structural models to obtain demand over capacity ratios (Y = D/C) of key bridge components that are processed statistically for each return period to determine the exceedance probabilities of specific limit states. These results are then used to fit continuous fragility curves for each bridge in the inventory.

The information obtained from the analysis is later processed to evaluate the efficiency and overall differences resulting from each IM through multiple bridge performance metrics. The selected metrics and their significance in terms of efficiency are presented in Table 1 and will be explained in further detail in the following sections. Finally, to illustrate how the different IMs could influence the estimates of roadway network interruption, a fictitious case study network is evaluated under a seismic event scenario to determine the number of bridges that could be tagged as inoperative. This output represents an additional indirect metric for the evaluation of the relative performance of the IMs.

3. Case study bridge inventory

3.1. Database description

A bridge database comprising 163 bridges from the National Autonomous Roads Corporation ANAS (*Azienda Nazionale Autonoma delle Strade)* inventory, collected and managed by the Eucentre Foundation (www.eucentre.it), was considered for the case study. These bridge assets form a part of the Italian road network and their geographic location is scattered along the primary highway grid of Italy, as shown in Figure 2. The information considered in the database comprises a practically complete account of geometrical, structural and material properties of the bridges, allowing a detailed structural numerical model of each asset to be created.

All the assets in the database are reinforced concrete (RC) bridges with simply supported beam-system decks, which is a predominant configuration in the Italian roadway network (Zelaschi, Monteiro, & Pinho, 2016; Borzi et al., 2015). Differences in the number of spans and pier types were used to define six bridge taxonomy branches, listed in Table 2. It is important to note that the taxonomy distribution of the bridges in the inventory is not uniform, i.e., some taxonomy branches include fewer assets than others, as shown in Figure 3(a). This must be considered when comparing taxonomy-based results, but it is to be expected given that the data represents a real existing inventory of bridges. Furthermore, the decision of dividing the bridges based on the number of spans in two categories, divided at the five-span threshold, could be considered somewhat ambiguous; however, it was determined in this way to allow for a similar amount of assets in both sides of the main taxonomy break, as seen in Figure 3(b).

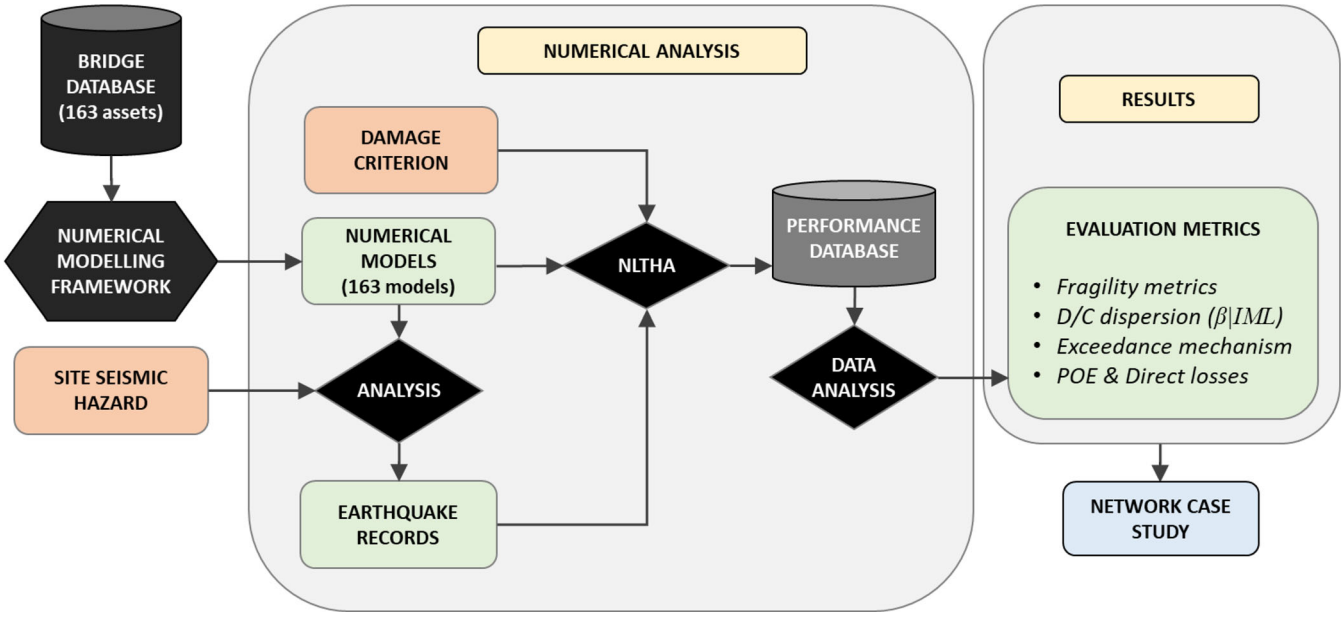

Figure 1. Methodology defined to produce fragility curves for main taxonomies.

Table 1. Selected performance metrics to evaluate IM efficiency and result comparison.

Performance Metric	Significance
Fragility curve dispersion ($\beta_{\ln Y}$)	The dispersion parameter of the continuous fragility curves can be seen as an indicator of efficiency since lower values of $\beta_{\ln Y}$ imply a higher probability of reaching a limit state for a given IM level.
D/C dispersion ($\beta_{Y\|IML}$)	The dispersion in the demand over capacity ratios obtained for each return period represent a direct indicator of IM efficiency, the lower dispersion associated with an IM the smaller number of records is required to capture the behaviour.
Exceedance mechanism	Though not a measure of IM efficiency, it was deemed interesting to investigate if there were differences between the underlying phenomena that cause the exceedance of a limit state using records chosen for different IMs.
Probabilities of exceedance and direct losses	Thorough comparisons of the mean annual probabilities of exceedance of each limit state as well as the resulting average annual losses using both individual and taxonomy-based perspectives were made to evaluate the difference in the behaviour obtained by using different IMs.

Figure 2. Location of 163 assets in the ANAS bridge inventory considered for the case study.

Even though the real location of each bridge in the database is known, for this case study, they will all be treated as if subjected to the same seismic demands corresponding to a specific site hazard in a localised region. This is a simplification that has been made to reduce the extensive NLTHA burden, described in the following sections, and to evaluate all assets under the same ground motion set. In actual applications, the procedure could be repeated for the different asset sites or a more hybrid means of selecting the ground motions to consider the seismicity of multiple sites could be used (Kohrangi, Bazzurro, et al., 2017). Further detailed information about the distribution of general geometric and material properties of the bridges in the database can be seen in Figures 3 and 4. Divisions of reinforcement ratios are included through the differentiation between pier types.

3.2. Modelling framework

To efficiently implement a modelling framework to generate, analyse and process the great amount of bridge information present in the database, a state-of-the-art tool developed by the Eucentre Foundation, called BRI.T.N.E.Y (BRIdge auTomatic Nonlinear analysis based Earthquake fragilitY) (Borzi et al., 2015), was used. The tool creates finite element (FE) models for carrying out NLTHA with OpenSees (McKenna, Scott, & Fenves, 2010) and processes the results to characterise the structural response of each bridge.

The models are created using elastic frame elements for the deck and BeamWithHinges (Scott & Fenves, 2006) elements for the pier segments and the transverse beams. Deck connections were modelled using zeroLength elements and twoNodeLink elements were used for bearing devices within

Table 2. Definition of taxonomy branches based on key structural parameters.

Material	Static Scheme	Spans	Pier Type	Taxonomy Branch
Reinforced Concrete	Simply Supported	2 to 4	Multiple Column	RC-SS-2/4-MC
			Wall	RC-SS-2/4-W
			Single Column	RC-SS-2/4-SC
		Above 5	Multiple Column	RC-SS-5+-MC
			Wall	RC-SS-5+-W
			Single Column	RC-SS-5+-SC

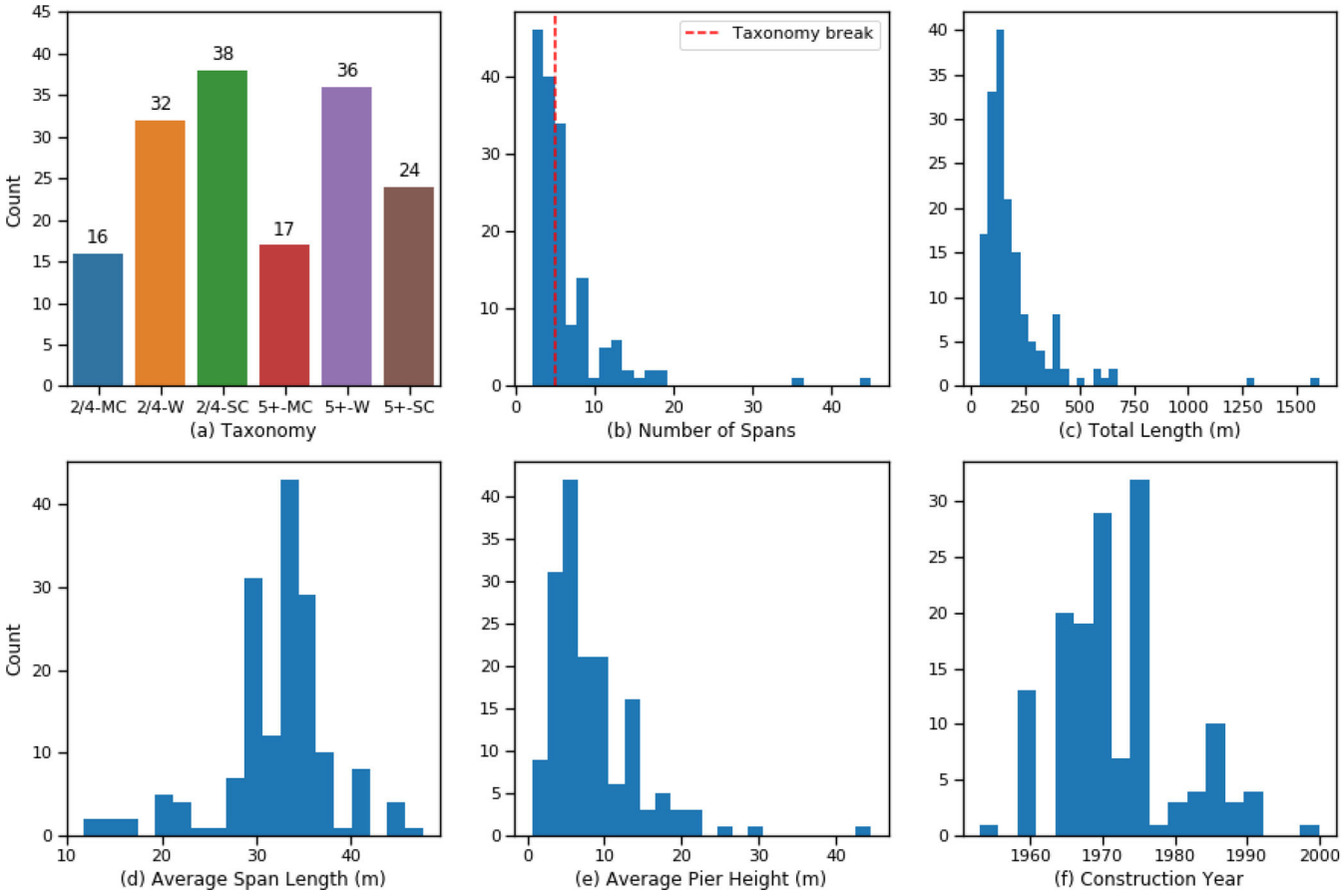

Figure 3. Distribution of general and geometrical properties of the bridge database.

super- to sub-structure connections. RigidLink elements are also used to model connection dimensions. Nonlinearity is modelled within both BeamWithHinges elements, where the cross-section is discretised into fibres, and zeroLength elements, where the non-linear relationships are calculated depending on the type of connection. Uniaxial constitutive models employed for the fibre section of inelastic elements are the Scott-Kent-Park concrete model (Kent & Park, 1971) (Concrete01 in OpenSees) and the bilinear steel model (Steel01 in OpenSees). Values for the material model parameters are established for each of them, based on the characteristic values of each material reported for each individual bridge, available in the database from blueprint specifications.

For the bearing supports and connections between the deck, piers and abutments, available force-deformation laws in OpenSees (e.g. Elastomeric, FlatSlider, FrictionPendulum) cover the full spectrum of devices, both traditional and modern, typically found in the bridge stocks of Italy. The platform also accounts for simple friction support between two surfaces simply supported, as well as monolithic connections. Even though the tool does allow for foundations and abutments to be explicitly modelled, the lack of the necessary data on the soil system did not allow exploring these aspects in this study.

However, this was not considered a major issue for the risk assessment of the bridge portfolios since most design practices require that the foundations be capacity-protected, which typically leads to significant conservatism in the design of bridge foundations (Chen & Duan, 2014). Furthermore, the tool allows for great flexibility in geometrical definitions to model bridges with complex layouts, such as having a curvature, multiple decks sharing piers, Gerber joints, etc. An example of the FE models created by the tool for a bridge from the case study portfolio is shown in Figure 5 and further information about the modelling framework can be found in Borzi et al. (2015).

3.3. Modal properties of case study bridges

Following the development of the numerical models for each asset in the inventory, a preliminary modal analysis

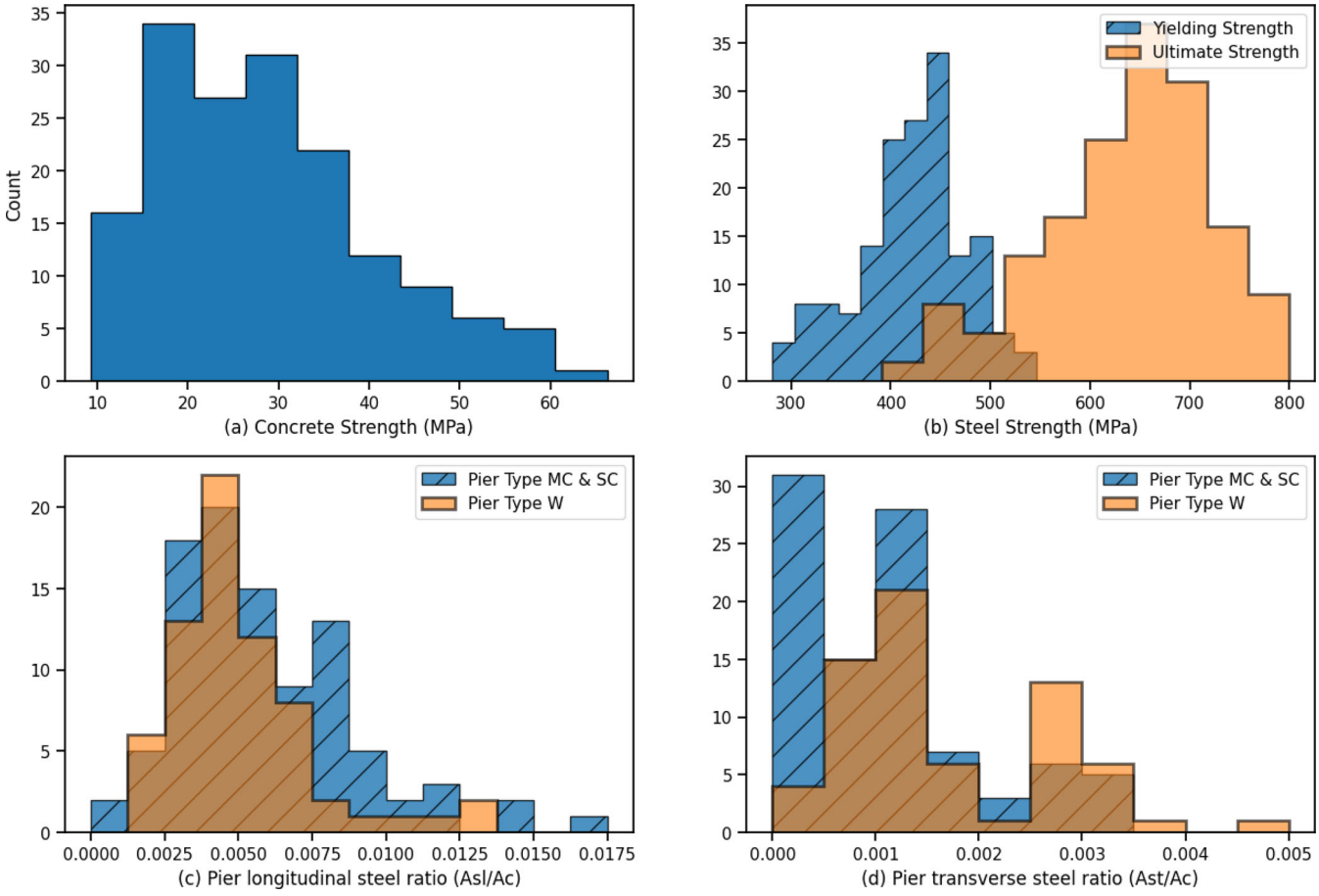

Figure 4. Distribution of main material properties of the bridge database.

was carried out to determine the first three structural periods of each bridge. The results from the modal analysis are shown in Figure 6(a), classified by taxonomy branch where the height of each bar represents the median period and the black lines the 95% confidence intervals of the data for each case to provide a measure of the period variability within the same group. It can be seen that the taxonomy branches that include more spans present higher overall medians and variations in all periods than their respective counterparts with fewer spans, an intuitive trend since larger bridges are expected to have longer oscillation periods in the transverse direction.

The aggregated results of the entire inventory are then used to determine an appropriate range of periods for the AvgSa IM record selection. While a study (Eads et al., 2015) has been made to determine the correct range of periods to use in AvgSa to reduce dispersion of the results, it dealt with the case of single buildings and therefore the recommendations are made in terms of the fundamental period (T_1) of the structure.

In the present study, given that there is no current recommendation for inventories of bridges, the lower limit was defined by 0.5 $T3_{median}$ and the higher limit as 1.5 $T1_{median}$, the intention being to use a lower bound that can include higher mode contributions and a higher bound that can account for period elongation in the non-linear range, for the majority of the case study bridges. This rule led to the selection of a range between 0.2 and 1.0 seconds, as shown in Figure 6(b), for the definition of the AvgSa record selection, which is considered adequate since it contains the vast majority of the period results for the assets in the database.

4. Seismic input definition

4.1. Probabilistic seismic hazard analysis

A site located in the northern part of the Campania region in Italy was chosen to carry out the PSHA required to select ground motion records. The OpenQuake engine (Silva, Crowley, Pagani, Monelli, & Pinho, 2014) was used to perform site-specific hazard calculations for both considered IMs, taking into account the soil category of the site. For this purpose, the Euro-Mediterranean Seismic Hazard Model (ESHM13) (Woessner et al., 2015), developed in the framework of the SHARE project, was adopted as reference seismic hazard model. The resulting hazard curves for the two chosen IMs are shown in Figure 7. A disaggregation analysis of the seismic hazard was also carried out to define the scenario events most contributing to the computed hazard levels.

4.2. Ground motion record selection

A selection of 30 two-component earthquake records (i.e., accelerograms) was performed for each of the nine considered return periods (30, 50, 98, 224, 475, 975, 2475, 4975 and 9975 years) giving a total of 270 ground motions for

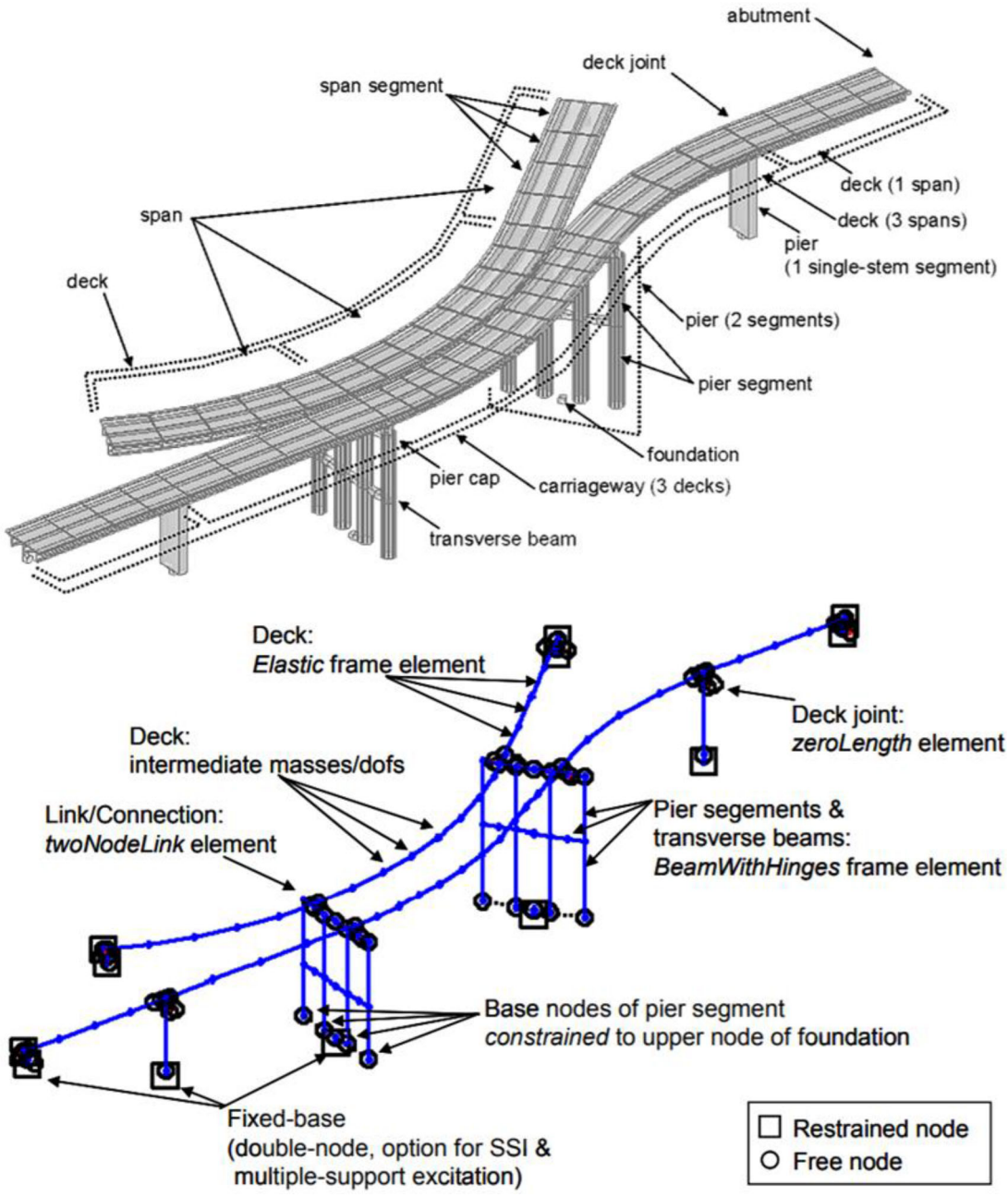

Figure 5. Example of a finite element model created using BRITNEY with the upper plot showing a simple rendering of the bridge system and the lower plot showing its discretisation within the numerical model. Adapted from Borzi et al (2015)

each IM. The selection process was carried out using a conditional spectrum (CS) approach (Lin, Haselton, & Baker, 2013) where a target response spectrum distribution (with mean and dispersion) is computed for each return period and IM. The original CS procedure was extended in Kohrangi, Bazzurro, et al. (2017) to define the target spectrum distribution also for AvgSa. A composite database made up by the PEER NGAWest2 database (Chiou, Darragh, Gregor, & Silva, 2008) and the Engineering-Strong Motion (ESM) database (Luzi et al., 2016) was then screened to preliminary select suitable recordings for the site under investigation.

In order to select and scale the records in a way that accurately accounts for their bi-directional characteristics, the RotD50 response spectrum (Boore, 2010) of each bi-directional earthquake recording was used to match compatible records with the target CS distribution selected for each return period–IM pair. This response spectrum comprises the median values of response spectra of the two horizontal components projected onto all nonredundant azimuths, both the PGA and AvgSa values of each record used was calculated in this space. An example of the response spectra associated to a set of selected accelerograms for the 475-year return period can be seen in Figure 8 for both PGA and AvgSa.

5. Fragility analysis

5.1. Damage criterion and limit states

Consistently with the BRITNEY analysis tool (Borzi et al., 2015) that was used to model and characterise the structural

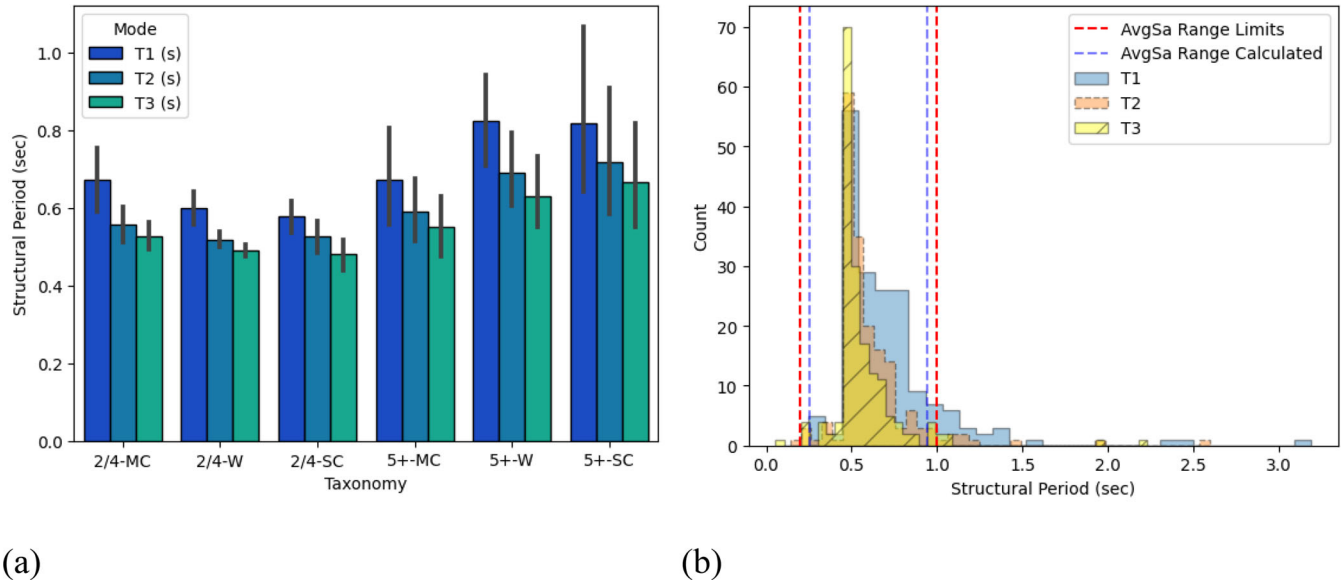

Figure 6. Results of the first three structural periods obtained from the modal analysis: (a) Divided by taxonomy branch, (b) definition of AvgSa period range.

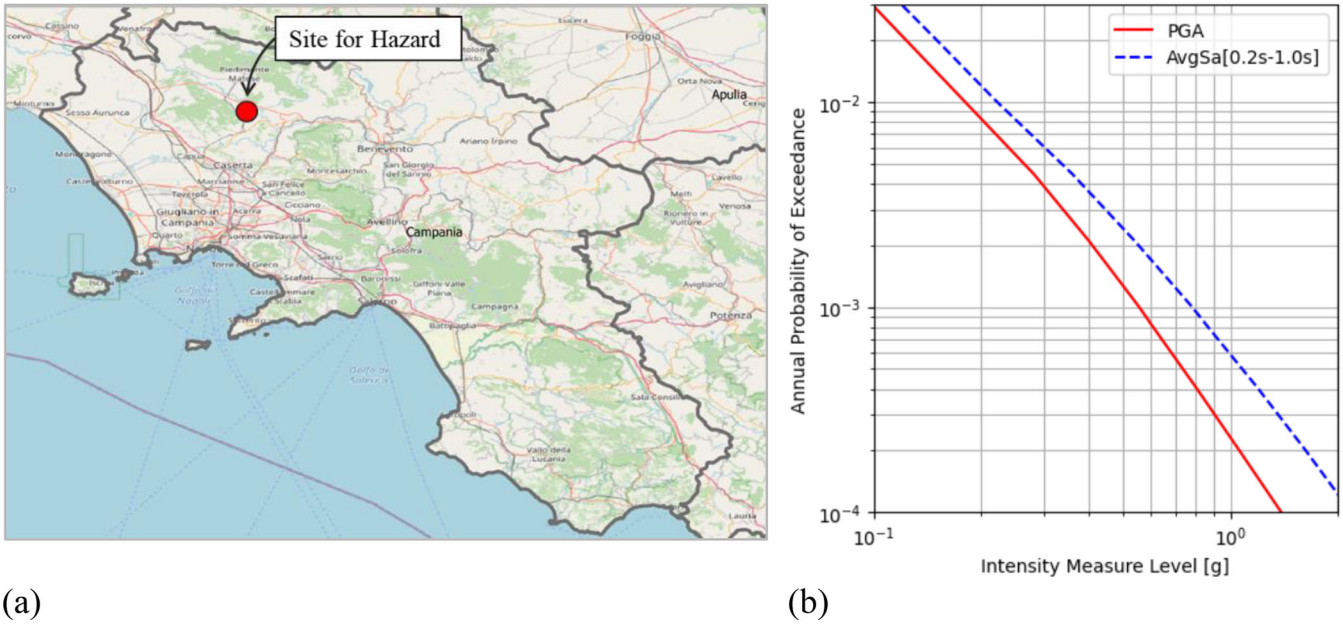

Figure 7. Site Seismic Hazard: (a) Site location, (b) Hazard curves for each chosen IM.

performance of the bridges in the database, two limit states were used for the evaluation of the performance of the assets: a) damage limit state, and b) collapse limit state. In this tool, structural deterioration interactions between elements leading to collapse are not specifically accounted for in the models (i.e. elements will deform beyond the limit response thresholds).

Instead of using explicit engineering demand parameters (EDP), a critical demand-to-capacity ratio per component ($y_i = d_i/c_i$) was used as damage measure to reflect how far each critical component is from the threshold of the limit state, which allows to later easily aggregate the state of its components into the global structural state (Jalayer, Franchin, & Pinto, 2007). Local demand over capacity ratios were calculated for piers and bearings and, depending on the values of these ratios, limit states were later assigned in the post-processing stage. In the case of piers, demand-to-capacity ratios were defined in terms of both chord-rotation and shear capacities. In terms of pier chord rotation, two response thresholds were considered: yielding of the section (θ_y) that was associated to the damage LS and, ultimate chord rotation (θ_u) associated to the collapse LS.

Yield and ultimate curvatures were determined automatically from a bilinear fit of a section moment-curvature analysis to deal with general cross-section shapes and reinforcement layouts. In terms of shear failure, given the brittle nature of the phenomenon, only a single threshold was defined and associated with the collapse limit state, with the pier shear capacity calculated according to the NTC 2008 equations (M.I.T., M.I., 2008). The shear span L_V was taken equal to the pier height L for single-stem cantilever piers, or in the longitudinal direction, and $L/2$ in the

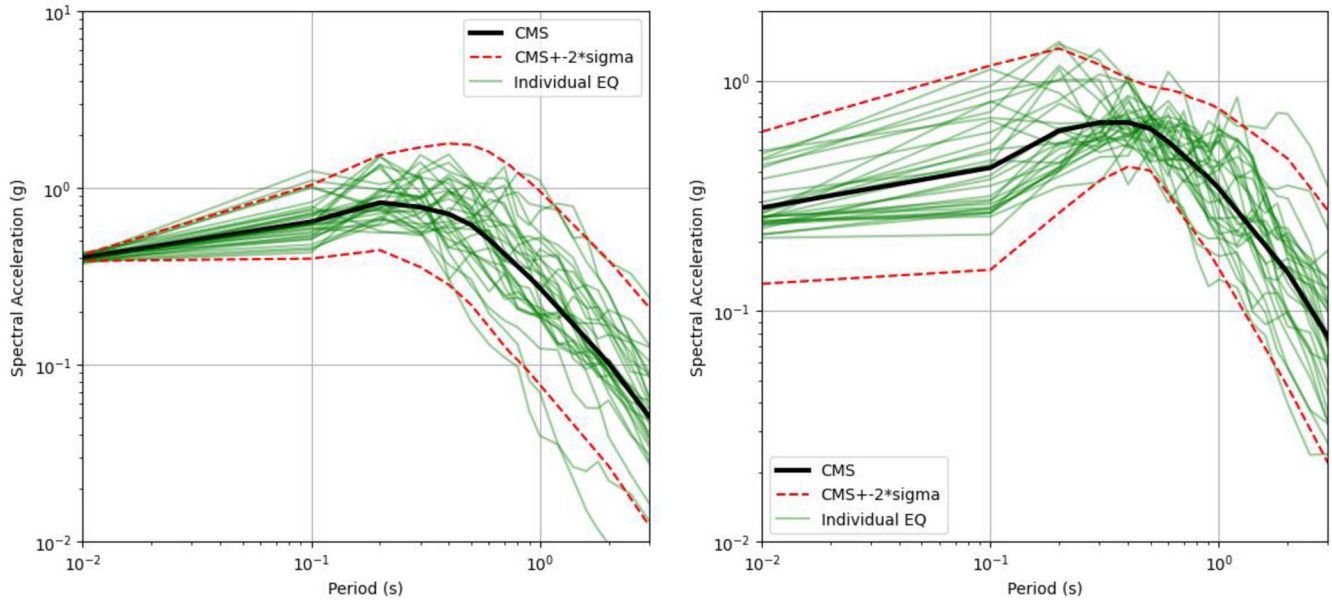

Figure 8. Record selection results for 475-year return period: (a) PGA, (b) AvgSa in the 0.2s – 1.0s period range.

transverse direction of multiple stem piers or piers with monolithic deck connections. Furthermore, to account for uncertainty in the capacity thresholds for pier components, these were modelled as lognormal random variables that were sampled every time an analysis was conducted. The equations used in the definition of the pier thresholds for chord rotation and shear, as well as the logarithmic standard deviation used for the analyses, are presented in Table 3. Further detail on the choice of the different formulations can be found in Borzi et al. (2015).

Regarding the bearings, demand-to-capacity ratios were calculated based on displacement demand. Two thresholds were defined: simple falling off the deck from the bearing seat, associated to the damage LS, and the full loss of support from the pier head, associated to the collapse LS. The displacement capacity of the bearings was derived from the pier cap and bearing seat geometry, or directly defined by the user, and was considered as deterministically known. To account for the bi-directional response under multi-component seismic input, the local D/C ratios, y_i, were taken as the SRSS combination for the piers and bearings, respectively. For example, the local ratio for flexural deformation at the collapse limit state was given in terms of the responses and capacities in the longitudinal (L) and transverse (T) directions as follows:

$$y_{i_{\theta_u}} = \sqrt{\left(\frac{\theta_{iL}}{\theta_{uiL}}\right)^2 + \left(\frac{\theta_{iT}}{\theta_{uiT}}\right)^2} \quad (1)$$

5.2. NLTHA and fragility curve definition

Each bridge model was evaluated using NLTH analysis to each set of 30 bi-directional records, for each of the nine increasing IM levels. Each individual record set provided a small sample of response corresponding to demand values D in each vulnerable component to be compared to its corresponding component capacity values C, sampled from their respective distributions. At each IM level, the obtained sample of the component demand to capacity ratios y = D/C was used to obtain a global, structural system level D/C ratio, denoted by Y (Jalayer et al., 2007).

Assuming that bridge components are a part of a series system, where the weakest failure system leads to the overall damage or collapse of the global structure, the global D/C ratio for the j-th intensity level and k-th ground motion is given in terms of the n local D/C ratios by:

$$Y_{jk} = \max(y_{1jk}, ..., y_{njk}) \; j = 1, ..., 9; \; k = 1, ..., 30 \quad (2)$$

The 30 values of Y at each intensity level were used to fit a lognormal distribution to determine the probability of exceedance of the unit value of Y that marks the attainment of the performance level being evaluated, as shown in Figure 9. These values of probability of exceedance form a piecewise fragility function, however, since a continuous function is desired for reference and ease of implementation in the platform, the points are assumed to follow a cumulative lognormal distribution.

A maximum likelihood estimation fitting algorithm (Baker, 2015) was employed to obtain the exponent of the logarithmic mean μ_{lnY} and dispersion β_{lnY} parameters that describe the fragility curve, as follows:

$$p(LS \mid IM : x) = \Phi\left(\frac{\ln\left(\frac{x}{\mu_{lnY}}\right)}{\beta_{lnY}}\right) \quad (3)$$

The process was repeated for each bridge model in a specific taxonomy and the results were processed statistically to obtain a class fragility function. For this purpose, the class lognormal mean is represented by the average of all the means of the bridge models, as presented in Equation (4), while the overall dispersion is given by the square root of the sum of squares of the intra-bridge dispersion and the inter-bridge dispersion:

Table 3. Capacity thresholds for pier segments (h and d_b are the section height and longitudinal bar diameter, respectively) adapted from Borzi et al. (2015).

Limit State	Mechanism	Median	Deviation $\sigma_{\ln}$
Damage	Flexure	$\theta_y = \frac{\phi_y L_v}{3}$	0.3
Collapse	Flexure	$\theta_u = \theta_y + (\phi_u - \phi_y) L_p \left(1 - \frac{L_p}{2L_v}\right)$ with: $L_p = 0.1L_v + 0.17h + 0.24\left(\frac{d_b f_y}{\sqrt{f_c}}\right)$	0.4
	Shear	$V_u = V_c + V_N + V_s$ with: $V_c = k(\mu_\Delta)0.8A_c\sqrt{f_c}$ $V_s = A_{st}0.9\ hf_y$ $V_N = N\frac{0.8h}{2L_v}$	0.25
θ_y : Yield rotation		V_u : Ultimate shear resistance	N: Axial load
ϕ_y : Yield curvature		V_c : Concrete shear resistance	fc: conc. compression strength
L_v : Shear length		V_N : Axial load contribution to shear resistance	fy: Steel yield strength
θ_u : Ultimate rotation		V_s : Transverse steel shear resistance	h: Section height
ϕ_u : Ultimate curvature		$k(\mu_\Delta)$: Ductility based reduction factor as per NTC2008	db: Bar diameter
L_p : Plastic hinge length		A_c: Concrete shear resistance area	

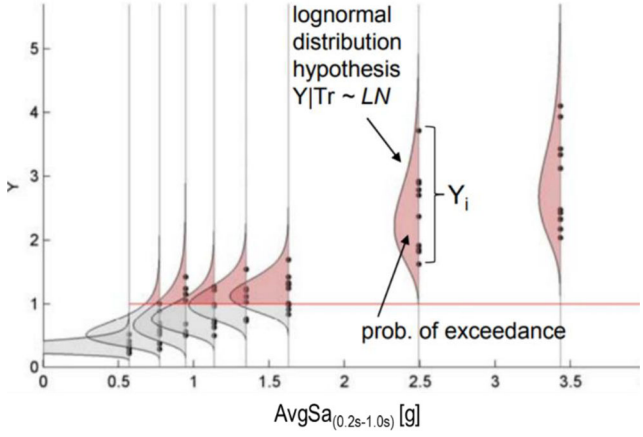

Figure 9. Sample values of the global D/C ratio Y being fitted with a lognormal distribution conditional on intensity level). Adapted from Borzi et al (2015)

$$ln\ \mu_{lnY_{tax}} = \frac{1}{N}\sum_{i=1}^{N} ln\ \mu_{lnY_i} \tag{4}$$

$$\beta_{lnY_{tax}} = \sqrt{\beta^2_{\ln Y_{intra}} + \beta^2_{lnY_{inter}}} \tag{5}$$

where:

$$\beta_{\ln Y_{intra}} = \frac{1}{N}\sum_{i=1}^{N} \beta_{lnY_i} \tag{6}$$

$$\beta_{lnY_{inter}} = \sqrt{\frac{\sum_{i=1}^{N}\left(ln\ \mu_{lnY_i} - ln\ \mu_{lnY_{tax}}\right)^2}{N}} \tag{7}$$

6. Results

6.1. Fragility metrics

Following the procedure described in the previous section, for each of the 163 case-study bridges, fragility curves for the damage and collapse limit states were defined as pairs of median (μ_{lnY}) and standard deviation (β_{lnY}) that define a lognormal distribution described by Equation (3), for both PGA and AvgSa. All resulting fragility curves, together with the calculated mean group fragility curves, are shown in Figure 10 for illustrative purposes alone since these mean curves include bridges from all taxonomy branches. Each individual curve was processed by grouping the results based on the taxonomy branch of each bridge leading to the taxonomy-based fragility curves described by the parameters shown in Table 4.

From these results, the value of dispersion (β_{lnY}) of the fitted fragility curve can be inferred to be representative of the relative performance of fragility curves calculated with different IM choices since lower values of dispersion are indicative of more abrupt changes between limit states, leading to more certain predictions of performance when compared to curves with higher dispersion values. Considering these assumptions and comparing the aggregated results obtained from each asset in the database, shown in Figure 11, it can be argued that the curves calculated using AvgSa as IM perform better in comparison to the curves calculated with PGA, as they present consistently lower dispersion values for both limit states.

The dispersion results were further investigated to determine if the values were sensitive to the taxonomy branch of each asset; in other words, the results were disaggregated per taxonomy branch and limit state, as shown in Figure 12. In this case, it can be seen that there is no apparent trend in the dispersion in terms of taxonomy branch. However, it can also be seen in both plots that, in general, the median dispersion values remain lower when AvgSa is chosen as IM when compared with their PGA counterparts.

6.2. Structural behaviour dispersion ($\beta_{Y|IM}$)

Another useful metric to evaluate the efficiency of an IM to characterise structural behaviour is the variability observed in the structural demands caused by records representative of the same return period that have been selected and scaled to have the same IM level (record-to-record variability). It is argued that a low variability of structural demand under such conditions is indicative of higher efficiency since it would require fewer records per IM level to capture the resulting behaviour.

As mentioned previously and illustrated in Figure 9, the demand over capacity ratios (Y = D/C) obtained from the NLTHA for each return period are fitted into a lognormal distribution that is used primarily to determine the probability of the structural demands exceeding a limit state threshold. Therefore, values of the median and dispersion

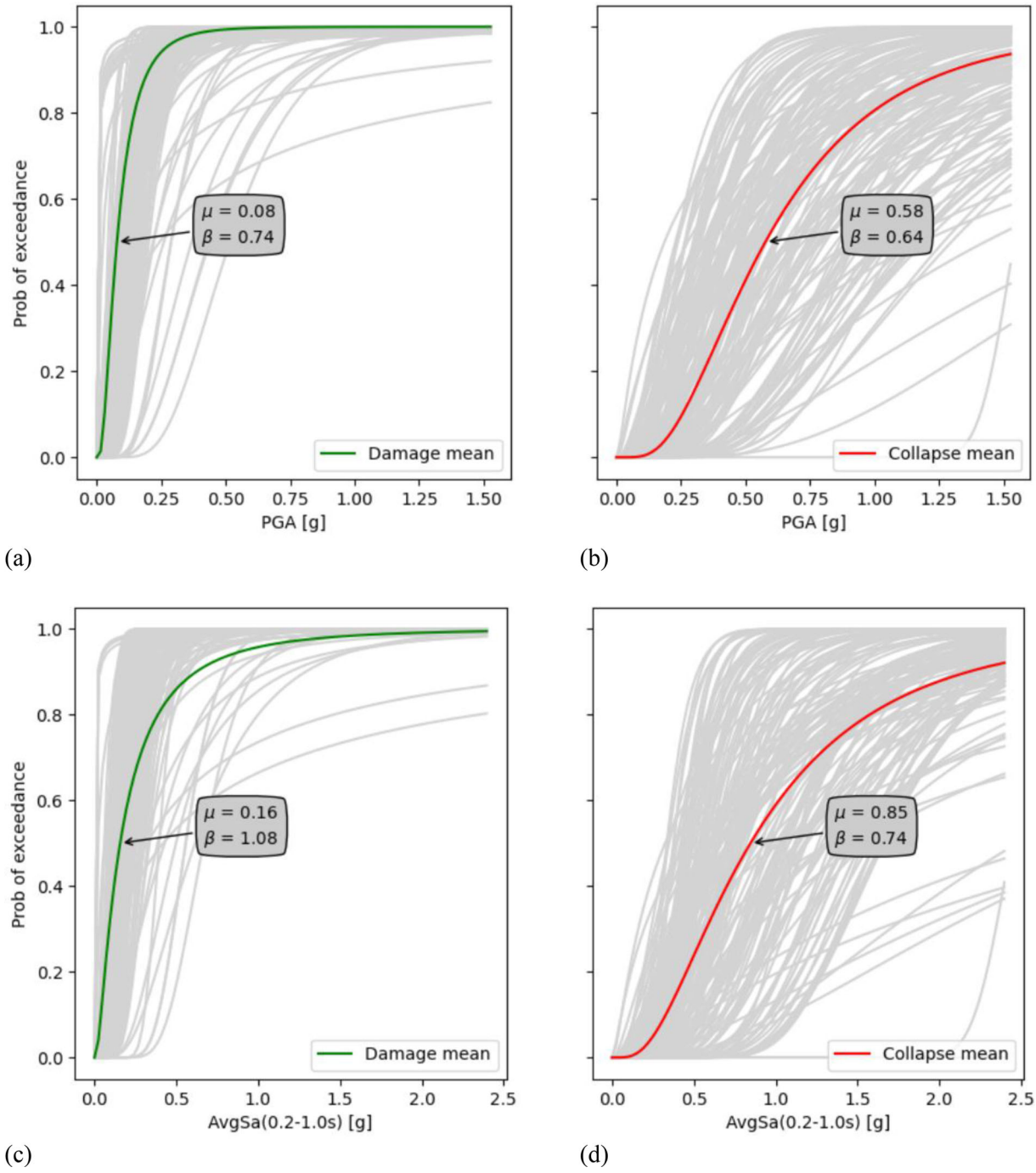

Figure 10. Fragility curve results obtained from NLTHA campaign on all 163 assets in the database for (a) Damage PGA, (b) Collapse PGA, (c) Damage AvgSa, (d) Collapse AvgSa.

Table 4. Taxonomy-based fragility curve results.

IM	AvgSa (0.2s-1.0s) [g]				PGA [g]			
Limit State	Damage		Collapse		Damage		Collapse	
Taxonomy	μ_{lnY}	β_{lnY}	μ_{lnY}	β_{lnY}	μ_{lnY}	β_{lnY}	μ_{lnY}	β_{lnY}
2/4-MC	0.185	0.731	1.131	0.540	0.076	0.992	0.694	0.621
2/4-SC	0.191	0.392	1.079	0.496	0.124	0.458	0.752	0.579
2/4-W	0.207	0.340	0.769	0.453	0.119	0.522	0.549	0.590
5+-MC	0.113	0.676	0.787	0.604	0.075	0.763	0.498	0.665
5+-SC	0.127	0.507	0.618	0.497	0.048	0.946	0.428	0.629
5+-W	0.122	0.539	0.847	0.672	0.049	0.960	0.582	0.740

per IM level are defined for each return period of which the dispersion value ($\beta_{Y|IML}$) is a direct indicator of the variability observed. These values were thus retrieved from the structural response database and plotted in terms of their corresponding return period, for both limit states and IMs evaluated.

The results obtained are shown in Figure 13, where the bold lines represent the median dispersions obtained from the entire inventory and the shaded areas represent the lower and upper quartiles observed per IML, included as a measure of variability. As it can be seen in Figure 13, the dispersion results for PGA and AvgSa show similar trends but with AvgSa always demonstrating lower median values for all return periods and both limit states considered, when compared with its PGA counterpart, leading to the preliminary conclusion that AvgSa is a more efficient IM choice.

6.3. Exceedance mechanism

As detailed previously, the NLTHA platform takes into account multiple EDPs to determine the probability of exceedance of a specific limit state, with each EDP being used to trigger a limit state based on the exceedance of either flexure, shear or bearing displacement (unseating) capacity. For simplicity, the fragility curve calculation was made with an enveloping approach, described in Equation (2), using the highest D/C ratios obtained throughout the NLTHA campaign for each exceedance mechanism in each asset analysed. However, to investigate the mechanism that contributes the most to the fragility of each bridge typology, as well as to determine if the IM choice has any influence in such a mechanism, the structural behaviour database was reanalysed to determine the most recurring mechanism that governs the fragility of each asset in the inventory.

The results of this exercise are shown in Figure 14, divided by limit state and taxonomy branch. It can be seen that the exceedance of flexure capacity is the governing mechanism for the majority of assets in all taxonomy branches and that the choice of IM for record selection has very little impact in the overall governing mechanism. This preliminarily indicates that the governing mechanism depends mostly on the particular characteristics (e.g., geometrical layout, materials, structural system) of each asset rather than the employed IM.

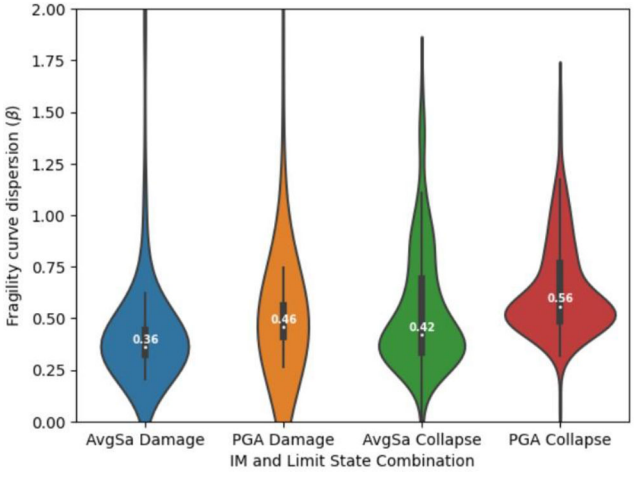

Figure 11. Fragility curve dispersion results for all assets, defined as a metric to evaluate the performance of IM choice.

6.4. Limit state probabilities of exceedance and direct losses

6.4.1. Probability of exceedance of limit states

To investigate the influence of the choice of IM in the probabilities of exceedance (POE) of the two limit states for different IM levels, the discrete results obtained from the NLTHA for the nine IM levels were associated with their respective return periods. This was to allow results from both PGA and AvgSa record sets to be plotted together and compared for each asset in the database. The aggregated results of all bridges in the database can be seen in Figure 15, where the bold lines represent the median values of POE for each limit state and return period observed for the entire inventory, while the shaded areas represent the lower and upper quartiles included as a measure of the corresponding variability.

It can be seen that the largest differences in the probability of exceedance between both choices of IM are present in the lower return period range of the Damage limit state, where the results obtained with the PGA selected records show a much higher median and uncertainty in the POE than its AvgSa counterpart. This trend is reduced for higher return periods as the Damage limit state becomes exceeded by the entire set of records above a return period of 975 years. In the case of the Collapse limit state, as it is shown in Figure 15(b), both IM choices lead to similar median results although, again, the PGA calculations yield a slightly higher POE for lower return periods than its AvgSa counterpart, a trend that is reversed for return periods above 2475 years.

Furthermore, by combining the POE results with the mean annual frequency of exceedance (MAFE) obtained

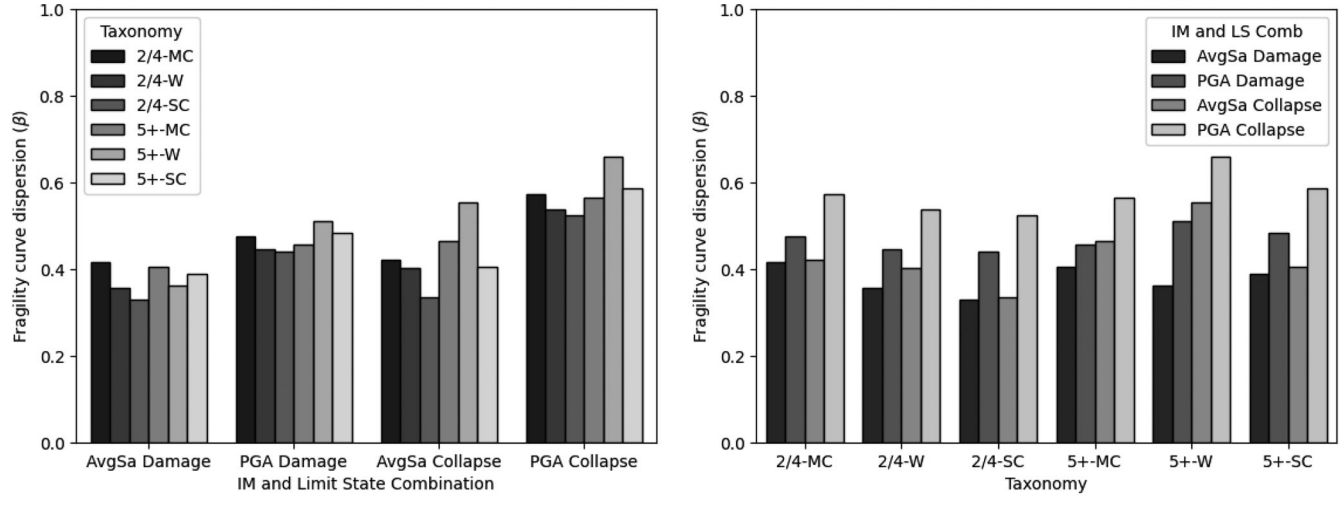

Figure 12. Median dispersion values obtained from the results of the entire database, represented in terms of (a) Taxonomy branch and, (b) Limit State.

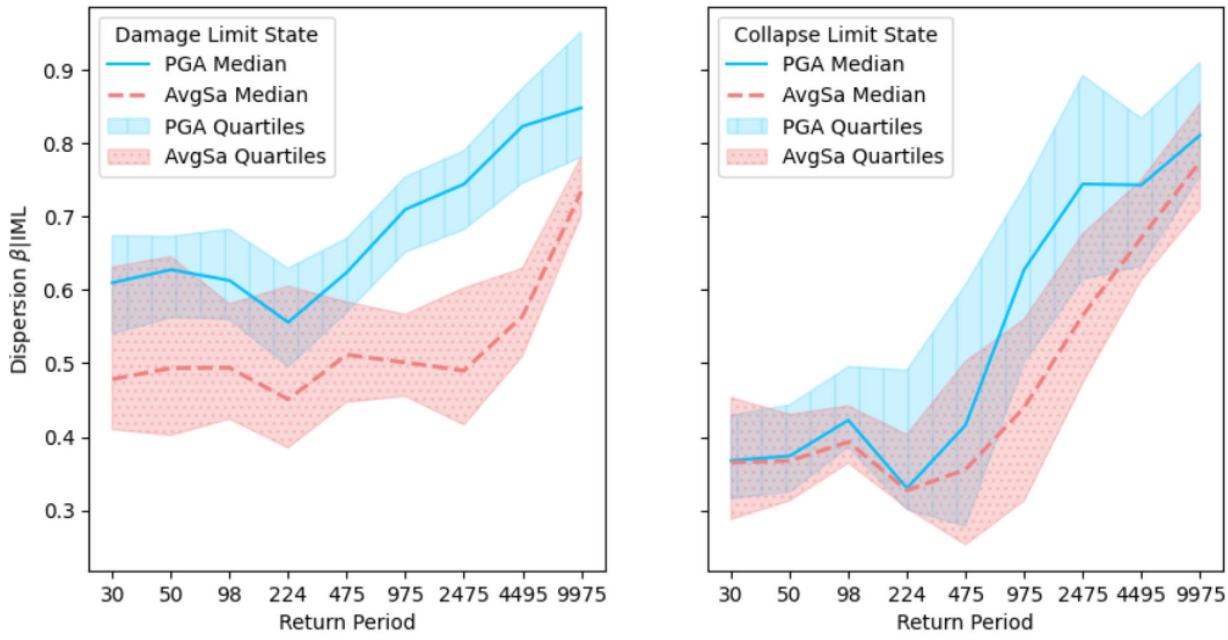

Figure 13. Dispersion of structural demand per IML obtained from the results of the entire database: (a) Damage Limit State, (b) Collapse Limit State.

during the hazard analysis for each IM level and integrating over the resulting curve, it is possible to obtain the annual probability of exceeding (APE) a specific limit state, as described schematically in Figure 16. This exercise was performed for each asset in the database and each IM choice for both limit states and the results are presented in Figure 17.

As it can be seen in Figure 17(a), when considering the entire inventory data, the median APE calculated with PGA as the IM was slightly higher for both limit states when compared to AvgSa. This trend was maintained when disaggregating the results by taxonomy branch, as shown in Figure 17(b), where it can also be seen that taxonomy branches representing bridges with more spans experience higher mean APE than their shorter counterparts with the same pier section types. This is considered an expected result since bridges with more elements are more likely to have any of them exceeding a specific limit state for an IM level.

6.4.2. Direct losses

Finally, a simplified methodology was adopted to evaluate the potential impact of the choice of IM on the direct economic losses that can be expected over the entire inventory. This methodology is based on the earlier versions of the Pacific Earthquake Engineering Research Center's Performance-Based Earthquake Engineering (PEER PBEE) framework (Porter, 2003) and it aims to calculate the direct Expected Annual Losses (EAL) for each asset in the database by accounting for the percentage of the replacement cost of the bridge associated to each limit state, also known as Mean Damage Factor (MDF), together with its probability of occurrence as described by:

$$\begin{aligned} \mathrm{EAL} &= \begin{bmatrix} p(\ LS_D) & p(\ LS_C) \end{bmatrix} \cdot \begin{bmatrix} €L|LS_D \\ €L|LS_D \end{bmatrix} \\ &= \begin{bmatrix} ((APE,\ LS_D) - (APE,\ LS_C)) & (APE,\ LS_C) \end{bmatrix} \\ &\quad \cdot \begin{bmatrix} MDF|LS_D \\ MDF|LS_C \end{bmatrix} \cdot €RC \end{aligned} \tag{8}$$

where:

LS_D: Damage Limit State	$APE,\ LS_D$: annual probability of exceedance of LS_D
LS_C: Collapse Limit State	$APE,\ LS_C$: annual probability of exceedance of LS_C
$p(LS_D)$: annual probability of occurrence of LS_D	$MDF\|LS_D$: mean damage factor for LS_D
$p(LS_C)$: annual probability of occurrence of LS_C	$MDF\|LS_C$: mean damage factor for LS_C
$€L\|LS_D$: direct economic losses associated with LS_D	€ RC: bridge replacement cost
$€L\|LS_C$: direct economic losses associated with LS_C	

For the present research, where the aim is to compare the impact of the choice of IM in these calculations, the MDF associated to the occurrence of LS_D and LS_C were considered deterministically known (no uncertainty was considered) and taken respectively as 8% and 100% of the replacement cost of each asset, which are the central MDF values indicated for Moderate Damage and Collapse limit state for bridges used previously in Perdomo, Abarca, and Monteiro (2020) and other studies conducted at PEER Center (Stergiou & Kiremidjian, 2008). Along the same lines, the replacement cost of each bridge was taken as proportional to the deck area, considering a generic cost per square meter. The EAL results, expressed as a percentage of the overall replacement cost of the entire inventory, are shown in Table 5.

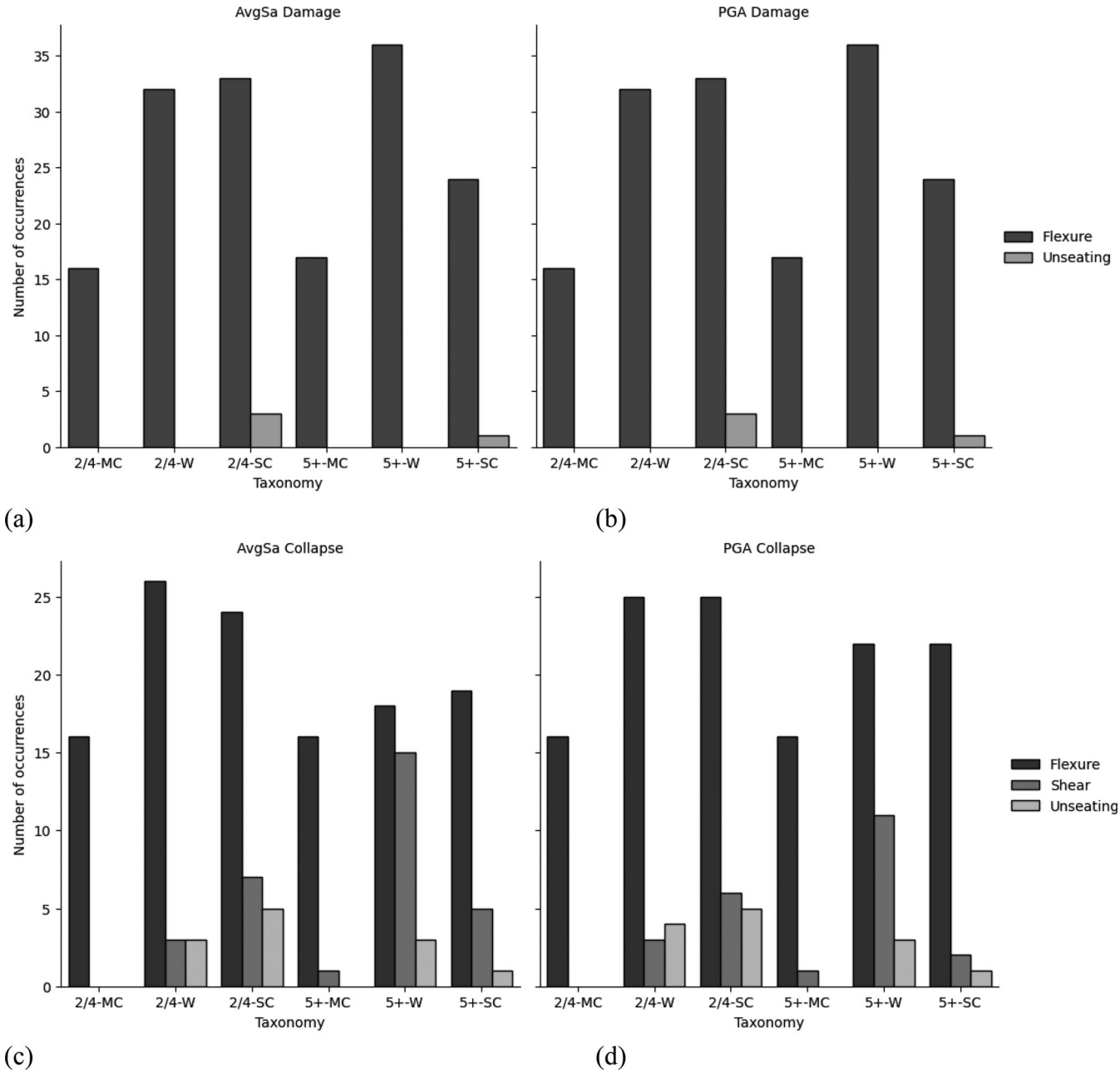

Figure 14. Structural mechanism that governs the exceedance of limit states separated by taxonomy branch for (a) Damage AvgSa, (b) Damage PGA, (c) Collapse AvgSa (d) Collapse PGA.

The EAL results obtained directly by using the probability of exceedance results from the NLTHA of each asset are presented in Table 5 as "EAL Individual," where it can be seen how the calculations made with the PGA sets lead to an increased estimation of EAL over the entire inventory when compared to the AvgSa sets, which can be attributed to the overestimation of POE and increased dispersion presented by the PGA results reported in Figure 17. It is worth noting that while this difference might seem small when considering the total cost of the inventory, the PGA estimate represents a 25% increase in EAL over the results obtained from AvgSa, which could represent a significant monetary value when referring to numerous bridge structures.

The EAL calculation exercise was also conducted using the POE derived from the taxonomy-based fragility curves assigned to each asset based on their corresponding taxonomy branch. This had the purpose of investigating the differences that can be expected when using taxonomy-based curves in regional bridge risk calculations compared to having individual curves for each asset. The results of this exercise are shown in Table 5 as "EAL Taxonomy-Based" where it can be seen that there were negligible differences between both calculations, leading to the preliminary conclusion that this type of analysis can lead to accurate results when evaluating risk metrics over the entire inventory. However, this conclusion does not hold true when considering the differences encountered between both calculations on an asset-to-asset level, where large variations can be found between results of a specific bridge if using the individual curve, when compared its taxonomy-based

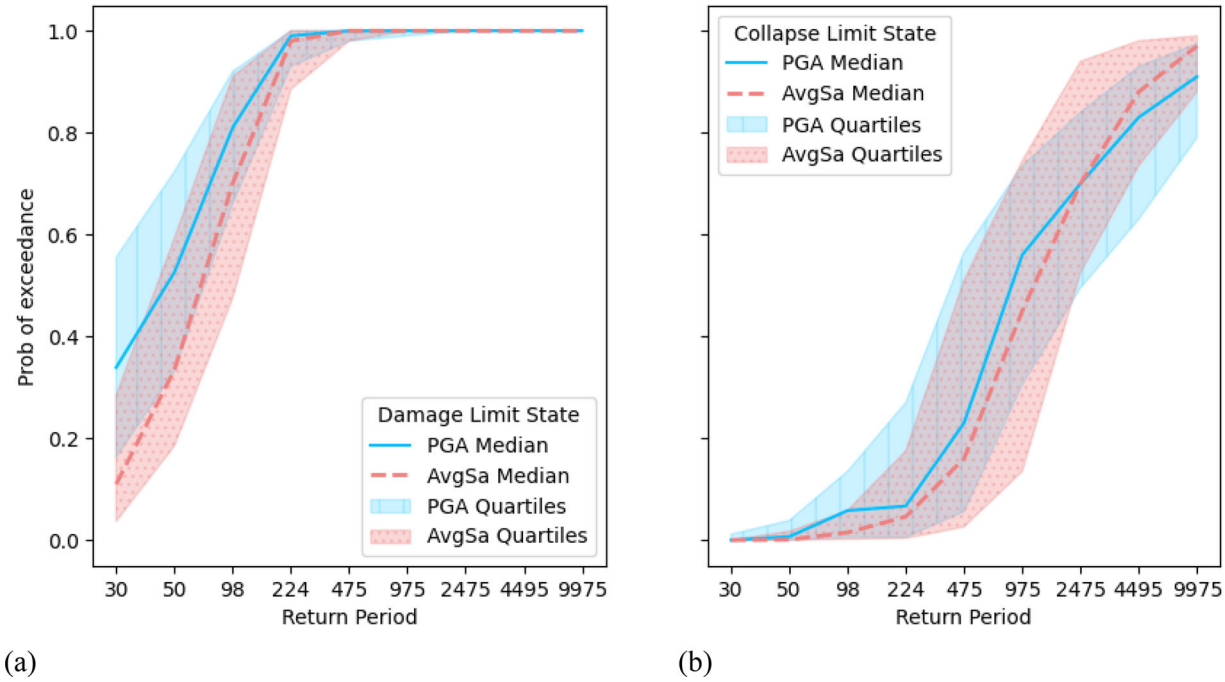

Figure 15. Probability of exceedance versus return period comparison for: (a) Damage Limit State, (b) Collapse Limit State.

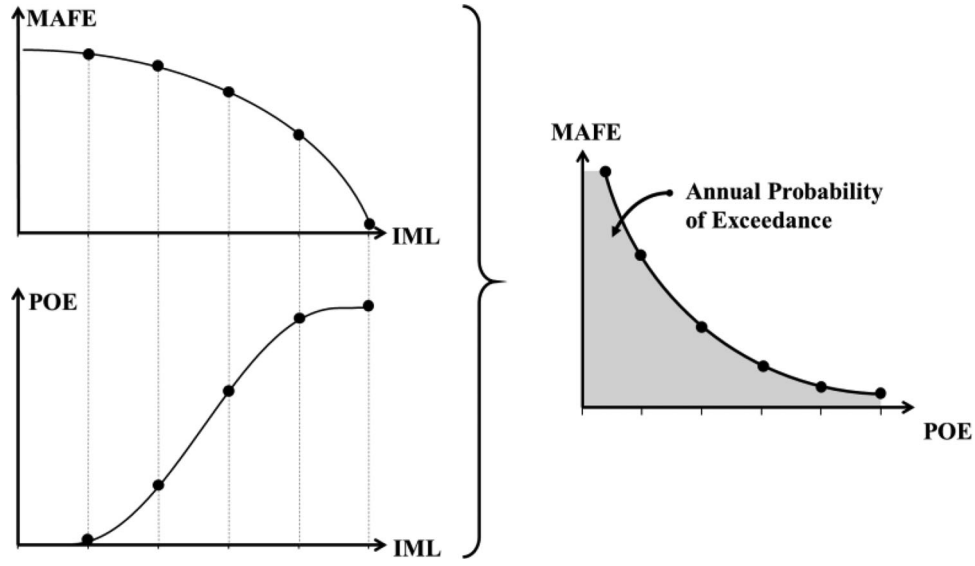

Figure 16. Schematic representation of the calculation of the annual probability of exceedance of a specific limit state.

counterpart, as shown in Figure 18, independently of the IM choice.

The results presented in Table 5 also allowed to evaluate the performance of the choice of IM in the definition of the taxonomy-based fragility curves themselves by considering the differences obtained in EAL for the entire inventory between the individual and taxonomy-based results within the same IM choice. It can be argued that the IM that leads to the smallest difference between individual and taxonomy-based results would represent a better IM choice for taxonomy-based evaluations, however, even though the AvgSa taxonomy-based EAL calculations did provide almost exact results compared to its respective individual-based counterpart (Ind/Tax = 99.6%), very similar results were obtained with the PGA set (Ind/Tax = 98.5%), therefore, both are deemed appropriate for this purpose.

7. Road network case study evaluation

A case-study scenario evaluation methodology, illustrated in Figure 19, was defined to assess the influence of the variability found in the results between fragility curves calculated with the different choices of IM in a spatially distributed scenario. In agreement with the methodology, a fictitious road network case study was defined by locating the bridges in the analysed inventory on the primary vehicular road system surrounding the hazard site. For this purpose, a database from OpenStreetMap OSM (OpenStreetMap contributors, 2020) was mined to extract the road network layer for the Campania region in Italy and select the location of 163 bridges of the primary network (highways and trunks) as shown in Figure 20.

The fragility properties of each of the original case study bridges were assigned to these locations, distributing the

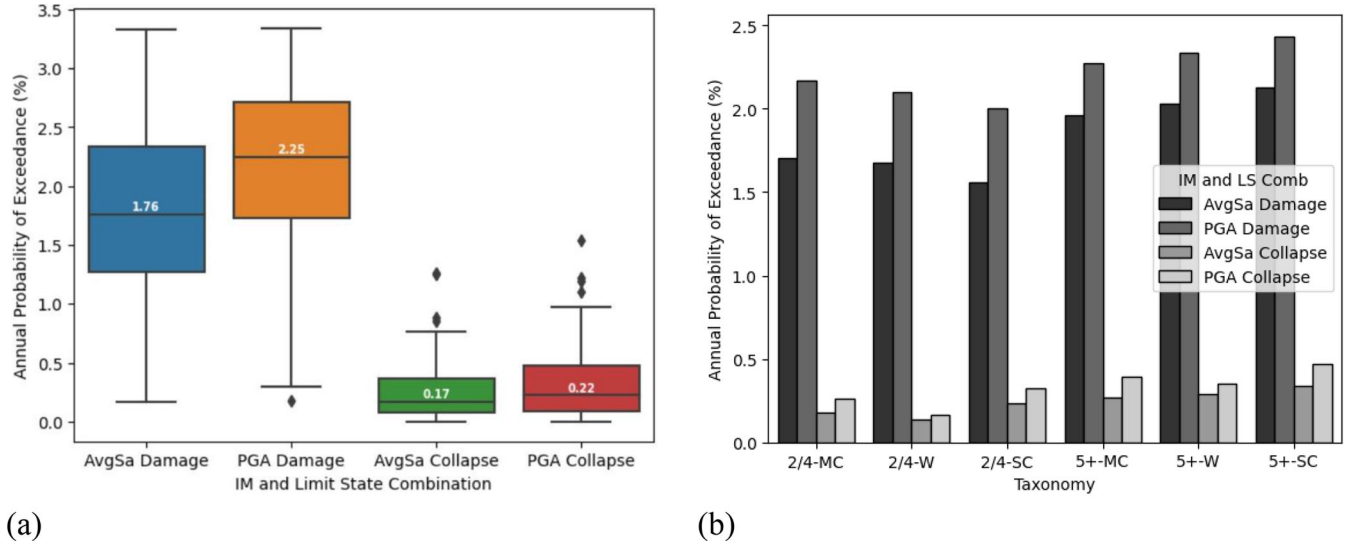

Figure 17. Annual probability of exceedance for each limit state and each IM choice: (a) aggregated results for entire inventory, (b) disaggregated results by taxonomy branch.

Table 5. Results for expected annual losses as a percentage of the replacement cost of the entire inventory.

IM	EAL Individual	EAL Taxonomy-Based	EAL Ind/Tax
AvgSa	0.406%	0.407%	0.996
PGA	0.513%	0.521%	0.985

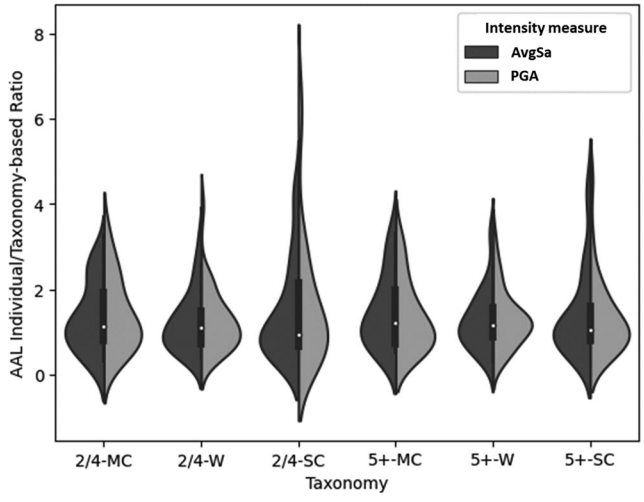

Figure 18. Ratio of EAL estimations made using individual fragility curve over taxonomy-based curves for each asset, divided by taxonomy-branch.

properties based on the sorted length of assets in both databases to minimize the total length difference between the OSM reported values and the assigned fragility curves. The differences between both length distributions are shown in Figure 21. A historical seismic event was used to evaluate the differences in road network disruption that can be predicted when using both choices of IM after an earthquake. For this purpose, the 1688 Sannio Earthquake that occurred on June 5th of 1688 in the vicinity of the hazard site location was chosen. This event, whose rupture information reconstructed from historical accounts (Bucci, Massa, Tornaghi, & Zuppetta, 2005) can be seen in Table 6, was estimated to have had a moment magnitude of 7.06 M_w and accounted for extensive destruction in the near areas, as well as an estimated 10,000 human casualties. This information was used as input to define an earthquake rupture model and perform a Scenario-Based Seismic Hazard Analysis (SSHA) using the Ground Motion Field Calculator available within the OpenQuake Engine (Silva et al., 2014).

For consistency with the hazard model used previously, the GMPE logic tree was replicated in these calculations and multiple realizations of ground shaking intensity were computed at the location of each bridge for the Sannio earthquake rupture. The mean values of shaking intensity obtained for each site and each IM choice are shown in Figure 22. Using these mean estimates of ground motion intensity, the probability of exceedance of the damage and collapse limit states were computed for each asset, considering both the PGA and AvgSa assigned fragility curves.

To determine if a bridge remains operational after a seismic event based on these probabilities of exceedance, threshold values of POE were defined for the damage and collapse limit states. This simplified methodology to flag unusable bridges in a scenario assessment based on thresholds has been previously used in research projects, such as INFRA-NAT (2018) and will be used herein to provide a notion on the differences that can be expected when using such methodology under both choices of IM considered. For the sole purpose of this academic exercise, it was defined that if any bridge in the case study that presented a POE above 90% for the damage limit state or 30% for collapse would be tagged as closed. These threshold limits, although somewhat arbitrary, are considered reasonable for comparison purposes, since the same thresholds are defined for both IM choices.

The results of bridge interruption can be seen in Figure 23, where 72 bridges exceeded the defined thresholds when using the fragility curves calculated for PGA as IM, in comparison to 59 closed bridges detected when using AvgSa. These results are in agreement with the findings in previous sections where metrics evaluated with the use of PGA as IM

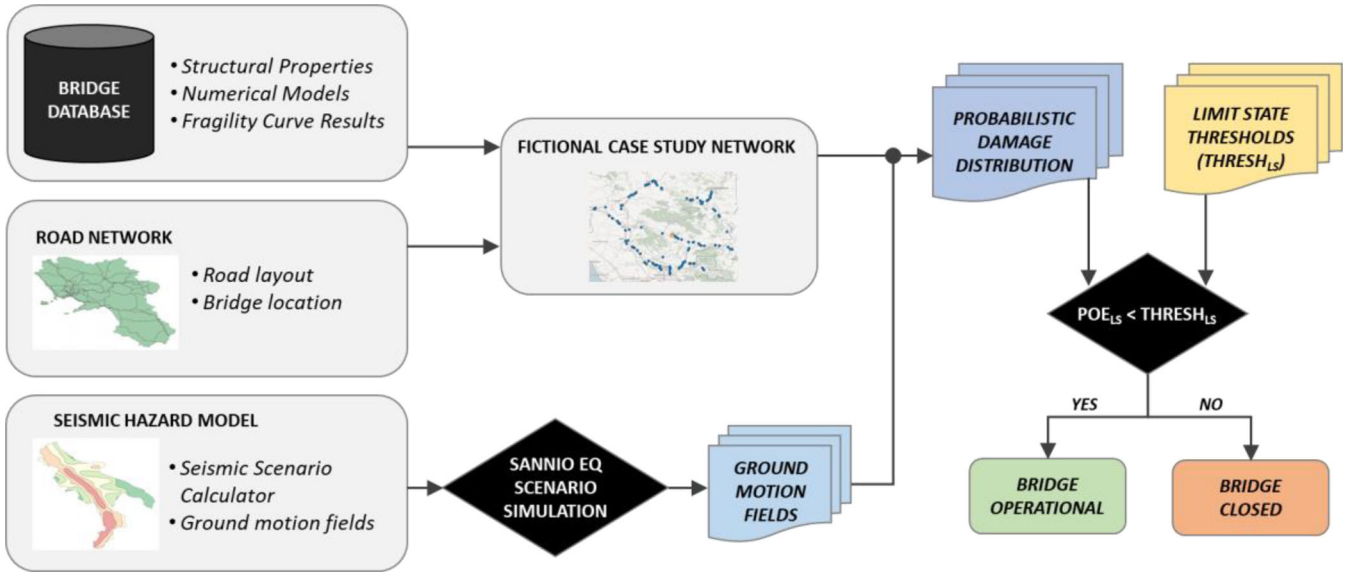

Figure 19. Methodology for the road network case study.

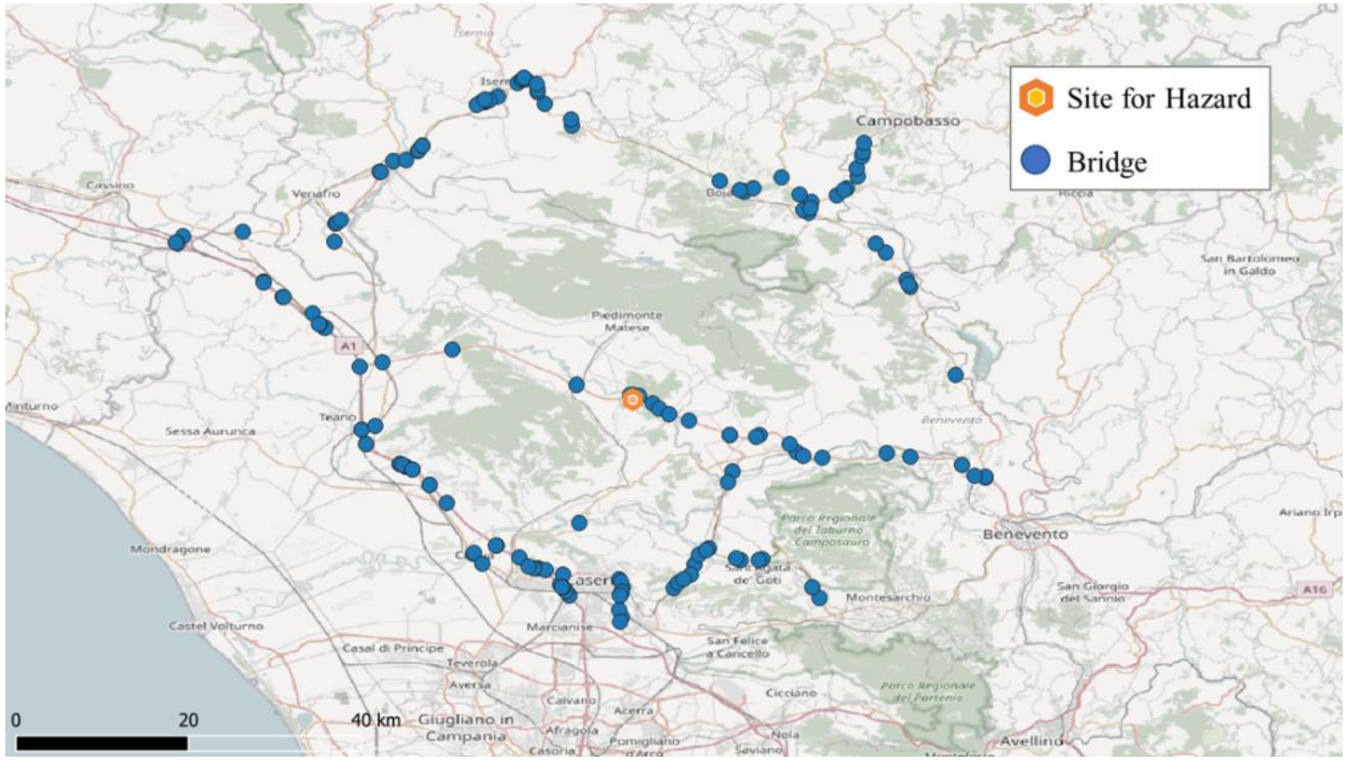

Figure 20. Fictional road network of the case study.

choice are consistently conservative when compared to the same values calculated with AvgSa.

8. Conclusions

In this study, a large inventory of existing reinforced concrete bridges with different configurations from the Italian road network was analysed through nonlinear time-history analysis (NLTHA) using hazard-consistent records, selected for both PGA and AvgSa as intensity measures (IM). Multiple fragility and vulnerability metrics were defined to compare the impact of the choice of the IM in the statistical and structural performance of a significant number of bridge assets from individual and taxonomy-based perspectives.

Based on the results obtained by the application of the methodology defined, the following conclusions can be drawn regarding the fragility estimates obtained by making different IM choices:

- From the statistical evaluation of dispersion values $\beta_{\ln Y}$ for the sets of fitted fragility curves, it is concluded that the use of AvgSa as IM consistently leads to fitted fragility curves with an overall lower dispersion in comparison to equivalent results calculated with PGA as IM.

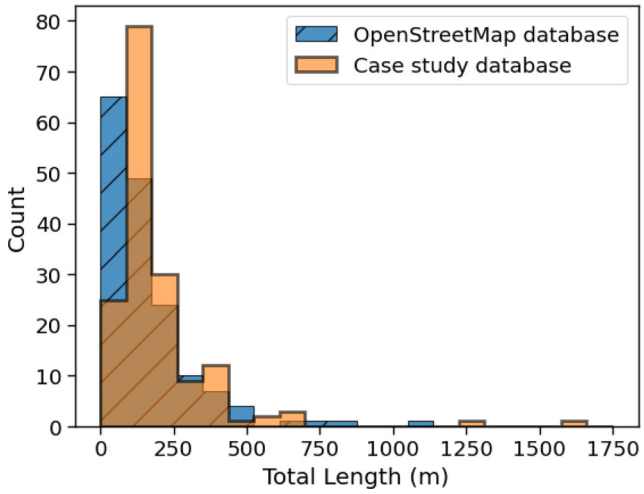

Figure 21. Distribution of total length between OSM and case study database.

Table 6. Input parameters for the 1688 Sannio Earthquake (Bucci, Massa, Tornaghi, & Zuppetta, 2005)

Latitude	41.283
Longitude	14.561
Moment Magnitude (Mw)	7.06
Fault mechanism	Normal
Depth	13 km

- In terms of structural response dispersion, given a certain IM level, based on the distribution of demand over capacity ratios obtained from NLTHA for multiple return periods and limit states, it was concluded that the use of AvgSa as IM leads to lower mean values of structural behaviour dispersion in comparison to results obtained using PGA as IM for all limit states and return periods considered, making AvgSa a more efficient choice for IM than PGA.
- Regarding the structural mechanisms that govern the fragility of different types of bridges for the NLTHA campaign performed, the flexure mechanisms were more recurrent than shear or unseating for all taxonomy branches and limit states considered, regardless of the choice of IM.
- The use of PGA as the choice for IM leads to conservative estimates of the probability of exceedance of all limit states considered, which in turn may lead to direct loss estimates that are in the range of 25% higher expected annual losses over the entire bridge inventory. This is an economically important outcome, as one can have a more accurate estimate of costs, particularly when having, for instance, limited resources with which to

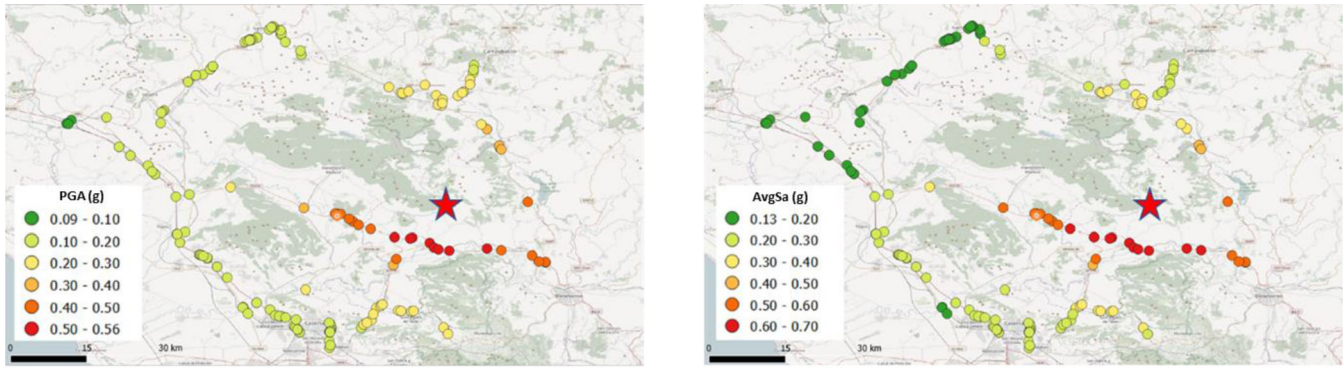

Figure 22. Results for ground shaking intensity obtained from the simulation of 1688 Sannio earthquake considering: (a) PGA, (b) AvgSa(0.2s-1.0s).

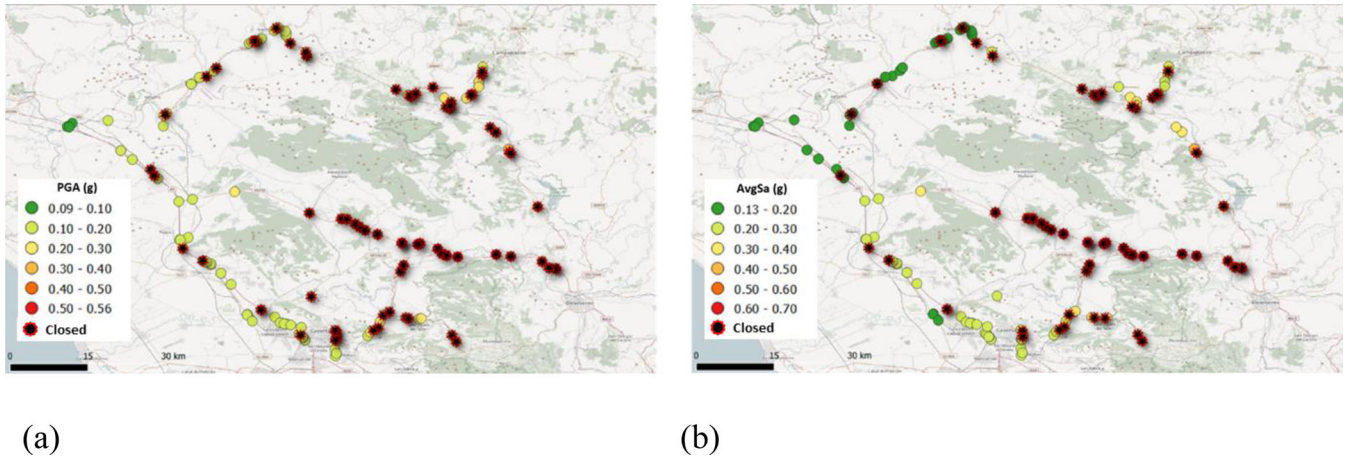

Figure 23. Results for bridge interruption obtained from the simulation of the 1688 Sannio earthquake, considering: (a) PGA, (b) AvgSa(0.2s-1.0s).

improve the seismic performance of the bridge inventory of a certain region.

- Calculations of average annual losses over an entire bridge inventory made with appropriately defined taxonomy-based fragility curves lead to almost exact overall results in comparison to calculations made with specifically calculated fragility curves for each asset in the inventory, regardless of the IM choice. However, large differences were observed at an asset-specific level and therefore it is not recommended to use taxonomy-based curves for a structure independent assessment.
- When performing the simplified exercise of assigning arbitrary but equal thresholds between choices of IM to detect closed bridges in a scenario-based case study, the use of PGA as the choice for IM lead to conservative estimates for road network interruption, which is in line with and confirms the observed trend on the probabilistic metrics that were analysed.

Overall, the outcomes of this study highlight AvgSa as an efficient IM over the more traditionally used PGA for regional seismic risk analysis, herein evaluated for the first time on a large inventory of real bridges with multiple structural configurations.

Disclosure statement

No potential conflict of interest was reported by the author(s).

Funding

The work presented in this paper has been developed within the framework of the project "Dipartimenti di Eccellenza", funded by the Italian Ministry of Education, University and Research at IUSS Pavia. It has also received support from the INFRA-NAT project co-funded by European Commission ECHO – Humanitarian Aid and Civil Protection. Project reference: 783298 – INFRA-NAT – UCPM-2017-PP-AG.

ORCID

Ricardo Monteiro http://orcid.org/0000-0002-2505-2996

References

Baker, J. W. (2015). Efficient analytical fragility function fitting using dynamic structural analysis. *Earthquake Spectra*, *31*(1), 579–599. Retrieved October 28, 2019, from https://earthquakespectra.org/doi/abs/10.1193/021113eqs025m doi:10.1193/021113EQS025M

Boore, D. M. (2010). Orientation-independent, nongeometric-mean measures of seismic intensity from two horizontal components of motion. *Bulletin of the Seismological Society of America*, *100*(4), 1830–1835. Retrieved July 23, 2020, from https://pubs.er.usgs.gov/publication/70041869 doi:10.1785/0120090400

Borzi, B., Ceresa, P., Franchin, P., Noto, F., Calvi, G. M., & Pinto, P. E. (2015). Seismic vulnerability of the Italian roadway bridge stock. *Earthquake Spectra*, *31*(4), 2137–2161. Retrieved January 18, 2019, from http://earthquakespectra.org/doi/10.1193/070413eqs190m doi:10.1193/070413EQS190M

Bucci, D., Massa, B., Tornaghi, M., & Zuppetta, A. (2005). Structural setting of the 1688 Sannio earthquake epicentralarea (Southern Italy) from surface and subsurface data. *Journal of Geodynamics*, *40*(2–3), 294–315. doi:10.1016/j.jog.2005.07.008

Carozza, S., Jalayer, F., Miano, A., & Manfredi, G. (2017). Probabilistic connectivity analysis for a road network due to seismically-induced disruptions. In *16th world conference on earthquake engineering*. Santiago, Chile.

Chen, W.-F., & Duan, L. (2014). *Bridge engineering handbook: Seismic design*. Retrieved October 25, 2019, from http://elib.polban.ac.id/index.php?p=show_detail&id=18431

Chiou, B., Darragh, R. B., Gregor, N., & Silva, W. J. (2008). NGA project strong-motion database. *Earthquake Spectra*, *24*(1), 23–44. Retrieved July 23, 2020, from https://journals.sagepub.com/doi/10.1193/1.2894831 doi:10.1193/1.2894831

DG-ECHO European Commission. (2017). *ITERATE Project*. Retrieved from ITERATE Project: http://www.iterate-eu.org/

DG-ECHO European Commission. (2018). *INFRANAT Project*. Retrieved from http://www.infra-nat.eu/

Eads, L., Miranda, E., & Lignos, D. (2015). Average spectral acceleration as an intensity measure for collapse risk assessment. *Earthquake Engineering & Structural Dynamics*, *44*(12), 2057–2073. Retrieved June 5, 2020, from https://onlinelibrary.wiley.com/doi/abs/10.1002/eqe.2575 doi:10.1002/eqe.2575

Jalayer, F., Franchin, P., & Pinto, P. (2007). A scalar damage measure for seismic reliability analysis of RC frames. *Earthquake Engineering & Structural Dynamics*, *36*(13), 2059–2079. doi:10.1002/eqe.704

Kent, D., & Park, R. (1971). Flexural members with confined concrete. *Journal of the Structural Division*, *97*(7), 1969–1990. doi:10.1061/JSDEAG.0002957

Kohrangi, M., Bazzurro, P., Vamvatsikos, D., & Spillatura, A. (2017). Conditional spectrum-based ground motion record selection using average spectral acceleration. *Earthquake Engineering & Structural Dynamics*, *46*(10), 1667–1685. doi:10.1002/eqe.2876

Kohrangi, M., Vamvatsikos, D., & Bazzurro, P. (2017). Site dependence and record selection schemes for building fragility and regional loss assessment. *Earthquake Engineering & Structural Dynamics*, *46*(10), 1625–1643. doi:10.1002/eqe.2873

Lin, T., Haselton, C. B., & Baker, J. W. (2013). Conditional spectrum-based ground motion selection. Part I: Hazard consistency for risk-based assessments. *Earthquake Engineering & Structural Dynamics*, *42*(12), 1847–1865. Retrieved July 23, 2020, from http://web.stanford.edu/~bakerjw/publications/lin_et_al_(2013)_cs-based_gms_i,_eesd.pdf doi:10.1002/eqe.2301

Luzi, L., Puglia, R., Russo, E., D'Amico, M., Felicetta, C., Pacor, F., Lanzano, G., Zare, M. (2016). The engineering strong-motion database: A platform to access pan-European accelerometric data. *Seismological Research Letters*, *87*(4), 987–997. Retrieved July 23, 2020, from https://pubs.geoscienceworld.org/ssa/srl/article-abstract/87/4/987/314138/the-engineering-strong-motion-database-a-platform doi:10.1785/0220150278

M.I.T., M. I. (2008). *NTC 2008 - Norme Tecniche per le Costruzioni (in Italian)*. Rome.

McKenna, F., Scott, M., & Fenves, G. (2010). Non-linear finite-element analysis software architecture using object composition. *Journal of Computing in Civil Engineering*, *24*(1), 95–107. doi:10.1061/(ASCE)CP.1943-5487.0000002

Monteiro, R., Zelaschi, C., Silva, A., & Pinho, R. (2019). Derivation of fragility functions for seismic assessment of RC bridge portfolios using different intensity measures. *Journal of Earthquake Engineering*, *23*(10), 1678–1694. doi:10.1080/13632469.2017.1387188

OpenStreetMap contributors. (2020). OpenStreetMap planet dump. Retrieved from OpenStreetMap: https://download.geofabrik.de/europe/italy/sud.html

O'Reilly, G., & Monteiro, R. (2019). On the efficient risk assessment of bridge structures. *7th ECCOMAS Thematic Conference COMPDYN*. Crete Island, Greece.

Padgett, J. E., Nielson, B. G., & DesRoches, R. (2008). Selection of optimal intensity measures in probabilistic seismic demand models of highway bridge portfolios. *Earthquake Engineering & Structural Dynamics*, *37*(5), 711–725. Retrieved November 30, 2020, from

https://onlinelibrary.wiley.com/doi/abs/10.1002/eqe.782 doi:10.1002/eqe.782

Perdomo, C., Abarca, A., & Monteiro, R. (2020). Estimation of seismic expected annual losses for multi-span continuous RC bridge portfolios using a component-level approach. *Journal of Earthquake Engineering*, 1–27. doi:10.1080/13632469.2020.1781710

Porter, K. (2009). Cracking an open safe: More HAZUS vulnerability functions in terms of structure-independent intensity. *Earthquake Spectra*, *25*(2), 361–378. doi:10.1193/1.3106680

Porter, K. A. (2003). An overview of PEER's performance-based earthquake engineering methodology. Ninth International Conference on applications of statistics and probability in engineering. San Francisco, CA.

Scott, M., & Fenves, G. (2006). Plastic hinge integration methods for force-based beam–column elements. *Journal of Structural Engineering*, *132*(2), 244–252. doi:10.1061/(ASCE)0733-9445(2006)132:2(244)

Silva, V., Akkar, S., Baker, J., Bazzurro, P., Castro, J. M., Crowley, H., Dolsek, M., Vamvatsikos, D. (2019). Current challenges and future trends in analytical fragility and vulnerability modelling. *Earthquake Spectra*, *35*(4), 1927–1952. doi:10.1193/042418EQS101O

Silva, V., Crowley, H., Pagani, M., Monelli, D., & Pinho, R. (2014). Development of the OpenQuake engine, the Global Earthquake Model's open-source software for seismic risk assessment. *Natural Hazards*, *72*(3), 1409–1427. Retrieved July 23, 2020, from https://link.springer.com/article/10.1007/s11069-013-0618-x doi:10.1007/s11069-013-0618-x

Stergiou, E., & Kiremidjian, A. (2008). *Treatment of uncertainties in seismic risk analysis of transportation systems (PEER Report 2008/02)*. Berkeley, CA: Pacific Earthquake Engineering Research Center.

Woessner, J., Laurentiu, D., Giardini, D., Crowley, H., Cotton, F., Grünthal, G., Valensise, G., Stucchi, M., The SHARE Consortium. (2015). The 2013 European seismic hazard model: key components and results. *Bulletin of Earthquake Engineering*, *13*(12), 3553–3596. Retrieved 7 23, 2020, from https://link.springer.com/article/10.1007/s10518-015-9795-1 doi:10.1007/s10518-015-9795-1

Zelaschi, C., Monteiro, R., & Pinho, R. (2016). Parametric characterization of RC bridges for seismic assessment purposes. *Structures*, *7*(7), 14–24. doi:10.1016/j.istruc.2016.04.003